An Acad Bras Cienc (2022) 94(Suppl. 1): e20211586 DOI 10.1590/0001-3765202220211586
Anais da Academia Brasileira de Ciências | *Annals of the Brazilian Academy of Sciences*
Printed ISSN 0001-3765 I Online ISSN 1678-2690
www.scielo.br/aabc | www.fb.com/aabcjournal

GEOSCIENCES

Iceberg drift and melting rates in the northwestern Weddell Sea, Antarctica: Novel automated regional estimates through machine learning

MAURO M. BARBAT & MAURICIO M. MATA

Abstract: Global warming and its consequences on polar regions have been thoroughly discussed in recent times. One of those consequences is the freshwater flux and the associated cooling and freshening that result from iceberg melting. Despite the potential impact, large uncertainties exist resulting mostly from the complexity to follow icebergs from space, which make the few existing estimates essentially model-based. This study takes advantage of state-of-art machine learning methods to present novel prevalent trajectories and potential freshwater input from 450 icebergs ranging from 1 to 2765 km^2 across the northwestern Weddell Sea, Antarctica. The main results highlight the predominance of a northward flux and the entrance of icebergs up to 10 km^2 into Bransfield Strait associated with the main current systems along the Antarctic Peninsula. The present analysis on such a large number of icebergs unveils an average drift speed of 3.4 ± 2.7 km day^{-1} and an average disintegration rate of ~62% per year, representing an integrated potential regional freshwater input of 133.62 Gt yr^{-1}. Altogether, this study adds new knowledge to the complex problem of autonomous applications for iceberg detection and tracking, further exploring such methods on a very dynamic region of singular importance for the ocean and climate studies.

Key words: icebergs, Southern Ocean, Antarctica, SAR, machine learning.

INTRODUCTION

Freshwater input via iceberg melting is an important component for the discussion of climate variability (Jacobs & Hellmer 1992, Jacobs 2004, Schodlok et al. 2006, Romanov et al. 2008). The dispersion of the cold freshwater from drifting icebergs (with areas from a few meters to thousands of square kilometers) through the polar ocean has the potential to disrupt temperature and salinity patterns far from their calving sites. For instance, sea ice formation is favoured where intense melting is observed as in those regions the freezing point of seawater is increased. Moreover, meting dilutes the surrounding seawater thus decreasing salinity and hence impacting bottom water formation rates due to reduced density of the source water masses. Finally, as a potential consequence of the previous process there is a slowing down of the deep convection rates in the source regions which affects deep ocean ventilation and ocean circulation (Schodlok et al. 2006, Romanov et al. 2008, Enderlin et al. 2016).

In the Southern Ocean, thousands of gigatons of icebergs are produced annually at the continental margins of the Antarctic Ice Sheet (AIS) (Jacobs & Hellmer 1992, Depoorter et al. 2013, Rignot et al. 2013, Barbat et al. 2019b) and their melt results in surrounding oceanic water masses dilution (Orsi et al. 1999, Gordon

2001, Kerr et al. 2012, Purkey & Johnson 2013, Starr et al. 2021). Gradually icebergs and the basal melting of the floating ice shelves around Antarctica constitute the two main freshwater sources to the Southern Ocean (Silva et al. 2006, Depoorter et al. 2013) able to impact the Antarctic Bottom Water (AABW) formation (Orsi et al. 1999, Kerr et al. 2012, Azaneu et al. 2013, Ferreira & Kerr 2017). Moreover, glacial bodies also have a marked influence on the cold and oxygen-rich (but also relatively fresh compared to the High Salinity Shelf Water) Weddell Sea Deep Water (WSDW) (One of the major components of the AABW), which highlights the special role of this Southern Ocean sector in the Meridional Overturning Circulation (MOC) (Bigg et al. 1997, Gladstone et al. 2001, Nicholls et al. 2009).

However, although the general impacts of icebergs melting have already been addressed by several studies, the knowledge about individual iceberg trajectories and melting is limited, partly due to the complexity of monitoring icebergs in the polar environment (Silva & Bigg 2005, Stuart & Long 2011b, Mazur et al. 2017, Collares et al. 2018, Barbat et al. 2019a, 2021).

Giant icebergs (larger than 18.5 km in length) have been systematically tracked by the U.S. National Ice Center (NIC) and the Brigham Young University (BYU) using scatterometer data (Stuart & Long 2011a). Conversely, smaller iceberg's drifting patterns have been generally restricted to ship observations, which are limited in space-time and susceptible to double sights (Jacka & Giles 2007), and space altimetry data limited to sea ice-free areas (Tournadre et al. 2016, Tournadre & Tarasenko 2019). Hence, currently, the few estimates existing of the spatio-temporally varying meltwater flux from icebergs smaller than 10 km^2 are mostly based on model simulations, still subject to high uncertainty (Gladstone et al. 2001, Merino et al. 2016, Stern et al. 2016, Rackow et al. 2017).

Recent studies have been proposed and debated about the positive synergy between Artificial Intelligence (AI) methods and Synthetic Aperture Radar (SAR) images for iceberg detection, tracking, and disintegration rates analysis (Mazur et al. 2017, Zhan et al. 2018, Barbat et al. 2019a, b, 2021, Hass & Jokar Arsanjani 2020, Rane & Sangili 2020, Rezvanbehbahani et al. 2020). While AI operates to improve detection performance over complex scenarios, SAR images have become a remarkable dataset for iceberg detection, allowing high spatial and temporal surveillance even during the polar night and independent of the prevailing cloud conditions (Williams et al. 1999, Gladstone & Bigg 2002, Silva & Bigg 2005, Wesche & Dierking 2012).

Altogether, this study discusses the prevalent iceberg trajectories and potential freshwater input across the northwestern Weddell Sea, Antarctica. The northwestern Weddell Sea region has been considered a climatic hotspot and has experienced extensive field efforts from the Brazilian oceanographic and climate research community in the last couple of decades. For this special volume: "Research in Antarctica – a tribute to Dr. Antonio Carlos Rocha-Campos", we chose this specific location to shed light on the iceberg presence and potential impacts for the region. In this sense, the combination of machine learning techniques and SAR imagery made it possible to identify and follow a large number of icebergs with surface areas from 1 to 2765 km^2, overcoming the usual limitation to giant icebergs (>340 km^2) which often restricts iceberg monitoring from remote sensing. The main results reinforce the predominance of a northward drift of icebergs in the northwestern Weddell Sea following the main current systems along the Antarctic Peninsula, the Antarctic Coastal Current (ACoC), Antarctic Slope Front (ASF) and, Weddell Front (WF) at an

average drift speed of 3.4 ± 2.7 km day^{-1}, with few small icebergs entering and circulating in Bransfield Strait. Finally, the computed average disintegration rate of ~62% year^{-1} leads to an estimated potential freshwater input of 133.62 Gt yr^{-1} for all tracked icebergs.

In the subsequent sections, we present the main regional oceanographic and glacial features for the northwestern Weddell Sea followed by a description of the data and methods used here. A detailed presentation of the novel results obtained, discussion, and conclusions complete this study.

WEDDELL SEA CIRCULATION AND GLACIAL FEATURES

The Weddell Sea (Figure 1, left panel) circulation is dominated by the cyclonic (clockwise) Weddell Gyre (Orsi et al. 1995, Su et al. 2014). The eastern coastal regime is dominated by the Antarctic Coastal Current (ACoC) and the western regime by the Slope Current, where the open-ocean water masses interact with the colder shelf waters and ice shelves (Fahrbach et al. 1992, Carter et al. 2008, Nicholls et al. 2009, Damini et al. 2021). Around the northern tip of the Antarctic Peninsula (Figure 2, right panel), the ocean circulation is characterized by a westward flow of the eastern side of the ACoC (flow coming from east) combined with the Antarctic Slope Front (ASF) and Weddell Front (WF), which are responsible for a strong barotropic northward

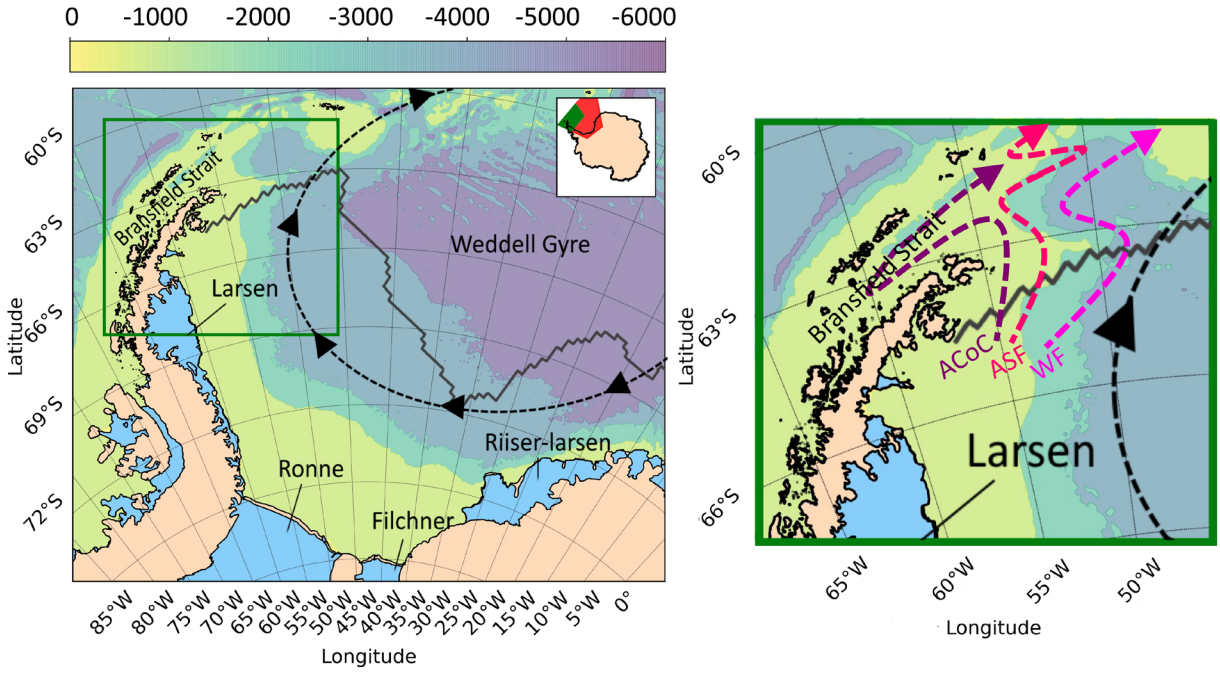

Figure 1. **Weddell Sea main features and circulation patterns. The schematics of the clockwise Weddell Gyre circulation are shown with a black dashed line (left panel). The average (minimal) sea ice extent in February (2002—2012) is shown with a dark grey line (https://nsidc.org/data/seaice_index/archives/). The bathymetry from the ETOPO database is also given by the color map; the main ice shelves in the Weddell Sea are depicted in light blue areas. The right panel shows an inset of the northwestern Weddell Sea area focus of this study, highlighting the northwestern Weddell Sea main circulation patterns: the Antarctic Coastal Current (ACoC- Purple dashed line), Antarctic Slope Front (ASF – red dashed line), and Weddell Front (WF- Pink dashed line).**

flow that is able to drag icebergs to the Powell Basin (and out of the Weddell Sea) or eastward into the ACC (Heywood et al. 1998, Stuart & Long 2011a). Confined by the Antarctic Peninsula to the south and the South Shetland Islands to the south, the Bransfield Strait is ventilated by different water masses following the ACoC through different routes across the complex topography near the tip of the Antarctic Peninsula (Dotto et al. 2016, Caspel et al. 2018, Damini et al. 2021).

The dominant glacial features in the Weddell Sea are the Filchner-Ronne and Larsen ice shelves, floating on the southern and western Weddell Sea continental shelves, respectively (Figure 1) (Nicholls et al. 2009). From these massive ice shelves, the prevailing cyclonic Weddell Gyre circulation guides icebergs northwestwards and into the Antarctic Circumpolar Current (ACC) domain, where the main iceberg velocity component becomes eastward (Merino et al. 2016, Rackow et al. 2017). From March to September, an approximately 1-m thick sea ice cover is formed in the Weddell Sea, which can extend to about 60ºS, e.g., (Schodlok et al. 2006). From October/November, the sea ice cover starts to retreat toward the Feb/March climatological minimum (Parkinson & Cavalieri 2012).

MATERIALS AND METHODS

Observing icebergs from space

The present study is based upon a selection of 627 C-Band (5.3 GHz, wavelength ~5.6 cm) ENVISAT medium-resolution Wide Swath Mode (WSM) Advanced Synthetic Aperture Radar (ASAR) images (pixel spacing 75m x 75m; 420km swath

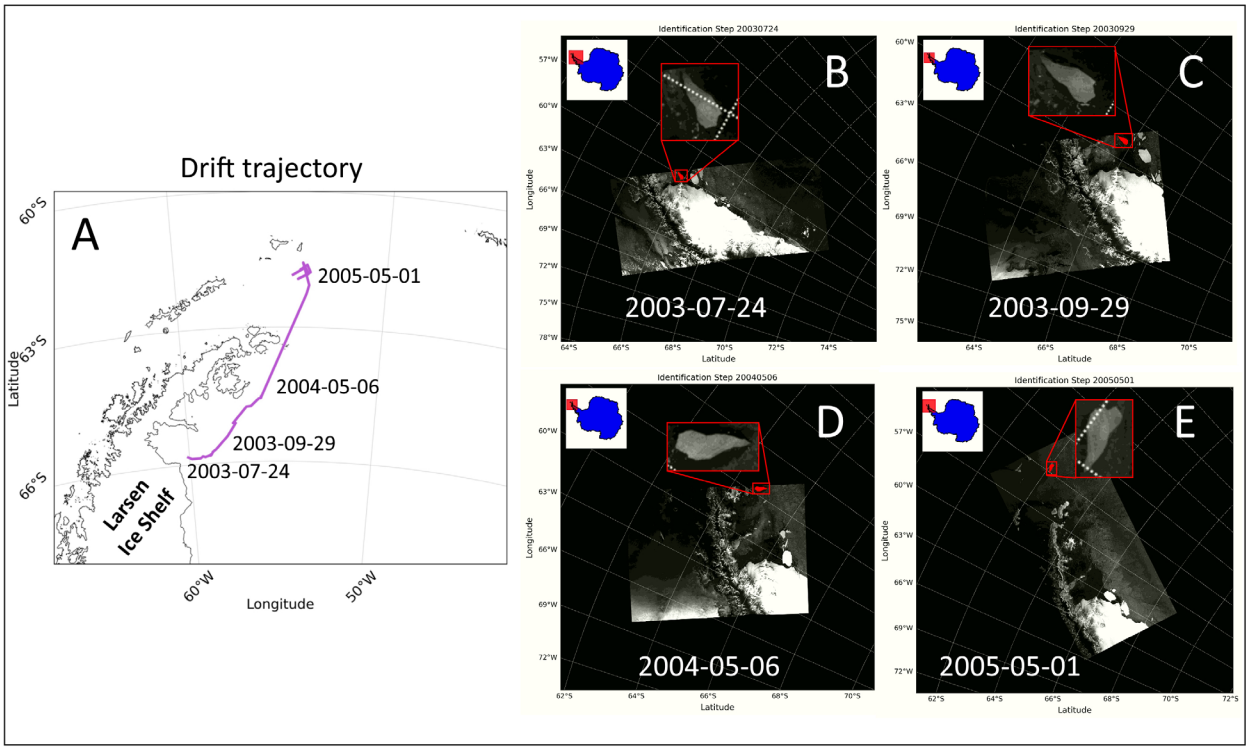

Figure 2. Autonomous detection and tracking exemplification. Panel A, trajectory estimated for a dark iceberg drifting from the southern tip of the Larsen-B ice shelf to the north of the Antarctic Peninsula between 2003, July and 2005, January. Panels B-E shows the tracked iceberg in four SAR images sampled along its trajectory with 33 re-detections.

width) (Envisat/ESA handbook 2007), acquired between 2002 and 2010 in the northwestern Weddell Sea. For iceberg detection and motion-tracking purposes, the complete dataset was initially calibrated, i.e., each pixel intensity can be directly related to the radar backscattering strength, re-projected (EPSG:3031 WGS 84 projection), and speckle-reduced applying a 3 x 3 Lee-sigma filter (Lee 1981). Then, the spatial overlap resulting from a large number of images with a wide strip of the covered ocean was used to revisit the same objects more frequently, improving the absolute revisit period of 35 days (Envisat/ESA handbook 2007) to 2-3 days.

Detecting and tacking icebergs with machine learning

Here, the machine learning methods presented in (Barbat et al. 2019a, 2021) are applied to iceberg detection and tracking from SAR imagery. For detection, we used a gradual learning flux (Incremental learning (Impoco & Tuminello 2015)) combined with the heterogeneous predictive model (Ensemble learning (Dietterich 2000, Polikar 2006, Marbach et al. 2012)), specialized in different iceberg properties observed in SAR imagery (Williams et al. 1999, Silva & Bigg 2005, Wesche & Dierking 2012). We achieved an average classification accuracy of 97.5 ± 0.6%, false positives rate of 2.3 ± 0.4%, and miss rate of 3.3 ± 0.4% respectively. Hence, the method proves to be a reliable alternative to extensive iceberg detection even in scenes where ambiguity poses major obstacles for autonomous detection.

In the next step, iceberg motion-tracking is performed by evaluating the pair-wise similarity between 1-D signals *f* and *g* (arrays) computed from spatial and morphological properties (i.e., area, perimeter, major-minor axis, and shape), using two similarity metrics and empirical relationships:

Jaccard index: measures the relationship between the number of sub-samples (subsets of integers) that are common to both signals over the total number of samples (Niwattanakul et al. 2013, Vorontsov et al. 2013, Santisteban & Tejada Carcamo 2015). It is defined as follows

$$j(f,g)=\frac{|f\cap g|}{|f\cup g|} \tag{1}$$

where $\cap$ determines common sub-samples between two signals *f* and *g*, and $\cup$ the total number of samples for both signals.

Cross-correlation: measures relative shifts between signal pairs (Zhang et al. 2003, Kohn 2005, Hale 2006), and it is defined by

$$c(u)=(f*g)(u)\equiv\int_{-\infty}^{\infty}f(x)\,g(x+u)\,dx \tag{2}$$

where u denotes the cross-correlation lag. For sorted signal pairs that are independent of the orientation of the icebergs, we can set $u=0$ (no lag).

Furthermore, to accept a pair match, empirical relationships are tested for (i) a minimum similarity threshold of 80% between iceberg pairs bigger than 3.4km^2 (Barbat et al. 2021) and 95% for smaller ones, (ii) a minimum length of 4 re-detections (number of detections in an individual trajectory), (iii) matched pairs must be within a maximum distance radius based on the average drift speed by size class (Bigg et al. 1997, Gladstone et al. 2001, Gladstone & Bigg 2002, Schodlok et al. 2006) and (iv) a maximum distance in days (two times the nominal time resolution of the SAR dataset used (< 70 days)). Although the empirical relationships are limited, they allow to remove obvious matching faults and, in addition, the conservative 95% similarity threshold for smaller icebergs allows to follow smaller icebergs with low shape variations between re-detection while 80% for large ones helps to avoid large-shape changes between

pairs, which can be either a real fragmentation or method flaw. For a complete description of both detection and tracking methods as well as method validations, we refer the reader to (Barbat et al. 2019a, 2021). We would like to note that for this study, although the dataset has been improved with new images to better represent the area of interest, the Envisat products (ASA_WSM_1P) and methods applied here are the same used and validated in the above-mentioned references. Hence, the validation for this study in addition to the applied visual inspection (e.g. Figure 2) is reliable.

Estimating iceberg mass and speeds

The iceberg mass is estimated based upon its horizontal surface properties calculated [in Gt] as

$$mass_{Gt} = \left(\left((NP_{pixels} - \frac{P_{pixels}}{2}) \times A_{m^2} \right) \times H_m \times \rho \right) / 10^{12} \quad (3)$$

where NP_{pixels} is the number of pixels identified as an iceberg unit, NP_{pixels} is the number of pixels of the iceberg outline (perimeter),A_{m^2} A_{m^2} is the typical physical area (m^2) covered by one pixel, H_m is the iceberg draft estimated by its empirical relationship with the iceberg major axis*(MjA)* (H_m = 2.91 x $MjA^{0.71}$) (Barker et al. 2004), and ρ = 850 kg m^{-3} is a typical density for icebergs in the Southern Ocean (Gladstone et al. 2001, Marino et al. 2015, Rackow et al. 2017, Barbat et al. 2019b). Half of the resulting perimeter is removed, since P_{pixels} represents a mixed signal between the iceberg and its surroundings.

Iceberg speed is estimated using the Euclidean distance in kilometers between the central position (in latitude and longitude) of consecutive samples for the same iceberg with a known date. To achieve a unit of velocity (km day^{-1}), the distance is divided by the elapsed time between the dates in days.

Estimating disintegration rates and potential freshwater input

Due to the variable elapsed time observed in each iceberg trajectory investigated, the disintegration rate is computed "per day" to standardize this parameter for all icebergs. To estimate an annual rate, the daily disintegration rates (p) were scaled up based on the concept of "daily compound interest", as

$$Annual_{rate} = \frac{A_{initial} - A_{after1year}}{A_{initial}} = 1 - \left(1 - \frac{p}{100}\right)^{365} \quad (4)$$

where $A_{initial}$ is a hypothetical initial surface area and $A_{after1year} = A_{initial} \times \left(1 - \frac{p}{100}\right)^{365}$ is the area after one year, assuming an area reduction of p [%] day^{-1} applied for a whole year (365 days).

The total iceberg mass loss is computed as the sum of all individual iceberg mass losses for nine years (2002-2010). Recall that each iceberg was followed for a different time interval (~70 days on average), so for a full year, the input will likely be larger. To estimate a potential freshwater input for a full year we considered the average number of "days followed" for all icebergs and scaled it up from the average days to a full year as:

$$Potential\ Freshwater\ input_{year} = \frac{Total\ mass\ loss}{9} \times \left(\frac{365}{average\ days\ following\ icebergs} \right) \quad (5)$$

RESULTS

Motion-drift estimates

Overall, 450 free-drifting icebergs with horizontal surface areas ranging between 1 and 2765 km^2 were investigated in the northwestern Weddell Sea between 2002 and 2010. The set of investigated icebergs can be subdivided into four classes as A2 (1-10 km^2) (256 icebergs, ~57%), A3 (>10-100 km^2) (145 icebergs, ~32%), A4 (>100-1000 km^2) (40 icebergs, ~9%), and A5 (>1000 km^2)

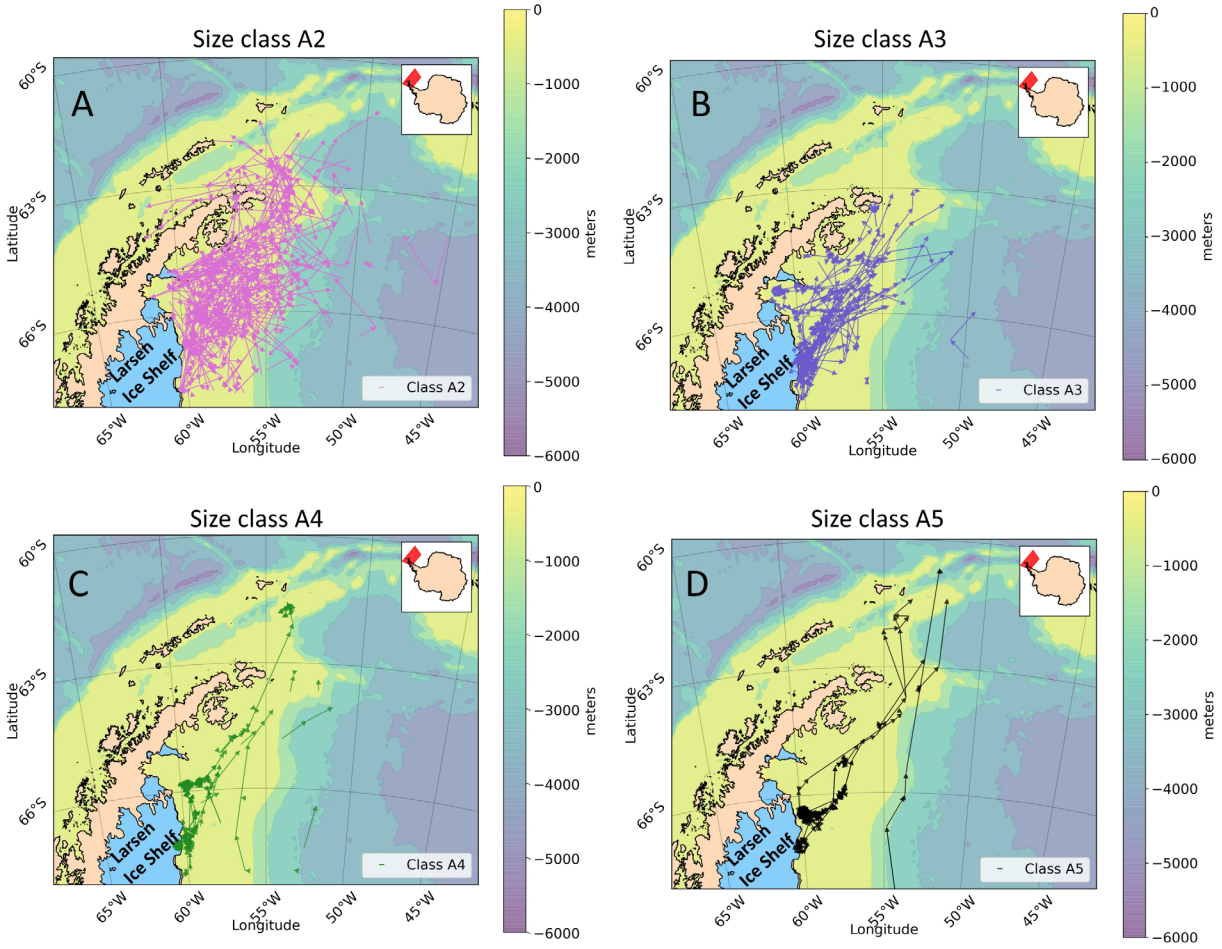

Figure 3. Trajectories for the 450 icebergs investigated in this study divided by size class. Size classes are subdivided by colors, purple for A2(1-10km^2), blue for A3(10-100 km^2), green for A4(100-1000 km^2), and black for A5 (>1000km^2). The color map depicts the bathymetry from the ETOPO database.

(9 icebergs, ~2%), respectively (Figure 3). Most of the monitored icebergs were first detected close to the Larsen Ice Shelf (hereafter called LIS), possibly as a result of the Larsen-B collapse in 2002. A major drifting pattern is present, with iceberg motion directed northward by the ACoC flow along the eastern Antarctic Peninsula (isobaths < 500m).

On average, the drift distance observed was ~178 km per iceberg and ranged from 0.22 km (for 1 day) to 1183 km (for 1839 days), with the average observation time for all icebergs being 70.02 days. The average iceberg speed was 3.4 ± 2.7 km day^{-1}, ranging from 0.15 to 25.3 km day^{-1}. The length of each trajectory in terms of the number of detection points varied between 2 and 136 (4.97 on average) per iceberg. The large variability observed in the main parameters can be associated with the large amplitude in size classes. In addition, although stationary icebergs have been removed, some icebergs may have become grounded in shallow areas and/or constrained by sea ice along their trajectory.

Of the nine giant icebergs belonging to the size class A5 (Figure 3, panel D), six possibly calved from LIS where they stayed close (first detection 2003), constrained by sea ice and/or bathymetry, for about 2 years before starting

to drift northward. From the remaining three of class A5, two bergs were first detected close to the tip of the Antarctic Peninsula in 2002, and the last one known as A22a, which entered the northwestern Weddell Sea sector in late 2004, originated from the vicinity of the Filcher-Ronne Ice Shelf further south. On average, A5 icebergs drifted 477 km at an average speed of 2.2 ± 1.5 km day^{-1} and were observed on average for 431.44 days. Similar to the trajectories observed for A5 icebergs, the A4 icebergs (40) (Figure 3, panel C) drifted northward usually with an initial detection close to LIS between 2002 and 2003 or came from the south. They drifted on average 119 km at 2.5 ± 2.1 km day^{-1} and have been observed for 95 days.

Overall, smaller size classes are more complex not only to follow the drift but also to try to relate such icebergs to a possible calving front. Due to the possibility of smaller icebergs being the result of fragmentation of bigger ones, the dispersion map becomes chaotic when compared to bigger size classes. For icebergs belonging to the size class A3 (145) (Figure 3, panel B), about one-third were first detected close to LIS. The average motion parameters for A3 icebergs resulted in 64 days of observation with 125.15 km of trajectory length at a speed of 3.1 ± 3.2 km day^{-1}.

Finally, for the 256 A2 icebergs (Figure 3, panel A) with surface areas between 1 and 10 km^2, although a general trajectory pattern is observed, it is not possible to relate those icebergs to a calving front clearly since a large number of those small icebergs can be the result of brittle fragmentation (bigger icebergs fragmentation) as discussed and modeled by (Åström 2006). Although it is interesting to observe that, differently from bigger classes, A2 icebergs often enter the Bransfield Strait following the ACoC with its rapid flow over the continental shelf and shelf-break. The tracked A2 bergs were followed on average for 52 days with a trajectory length of 200 km at a speed of 3.8 ± 2.2 km day^{-1}. On average the A2 icebergs were detected 3.8 times per trajectory ranging from 2 to 13 detections.

As noticed above, although not direct and linear, there is a visible correlation between area and observation time (Figure 4, left panel) and also between area and speed (Figure 4, right panel). The correlation (Pearson correlation) of 0.59 was computed between iceberg size (area) and observation time length. This makes sense mainly when considering that bigger icebergs are easier to detect and to follow and, in addition, their longer lifetime allows those bergs to be revisited in a larger number of SAR scenes, remaining present for years before the total disintegration. For area and speed, although a weak inverse correlation of -0.14 is present, meaning smaller icebergs drift faster than bigger ones. Those correlations must be taken carefully, the vast majority of the tracked icebergs are located within the averaged minimum sea ice extent, which means that small icebergs' speeds could be influenced by the sea ice drag as it grows toward its maximum extent. Additionally, stronger winter winds can also have a steering influence on icebergs' speeds (Lichey & Hellmer 2001, Schodlok et al. 2006). Finally, it is important to note that some icebergs may have become grounded in shallow areas and/or constrained by sea ice along their trajectory, influencing speed statistics.

Freshwater estimates from iceberg disintegration

The integrated initial mass for all icebergs in this study was 6801.37 Gt with an average disintegration rate of ~62% yr^{-1}. The latter leads to an estimated potential freshwater input of 133.62 Gt yr^{-1} (Equation 4 and 5). The spatial

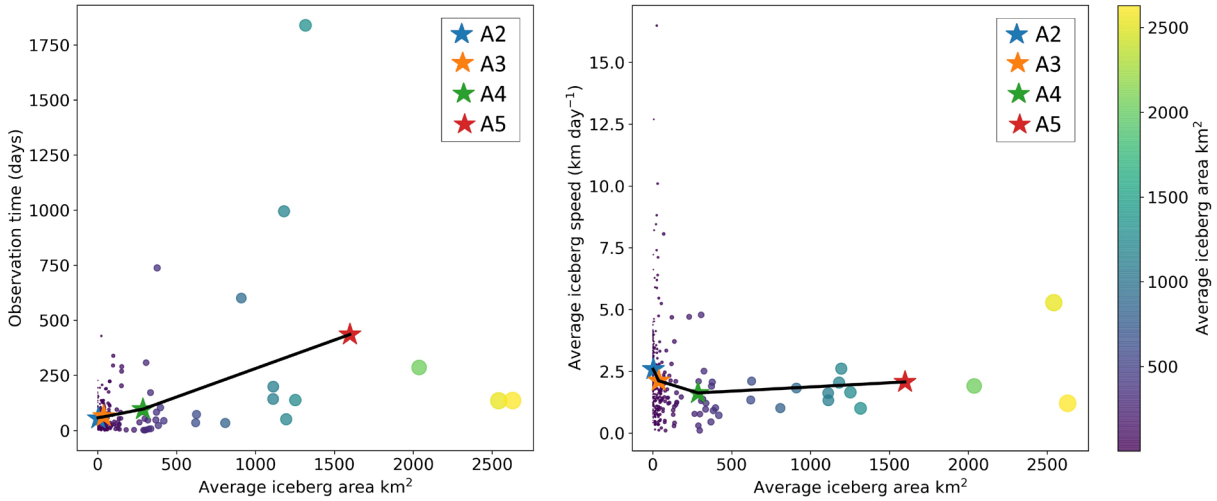

Figure 4. Relationship between area (km²) and total observed time length (days) (Left panel) and, the relationship between area (km²) and average drift speed (km day^{-1}) (right panel); for both panels circle sizes (and color) denote average iceberg areas (km²). Stars show the averages by iceberg size class and, the black line is a non-linear fitting between those averages.

mass loss distribution (per day) for all iceberg trajectories is shown in Figure 5.

Figure 6 (main panel) relates the total occurrence (y-axis, logarithmic scale) of each mass loss estimated due to a reduction in surface area. The annual mass loss estimated from area reduction between 2002 and 2010 is also shown in the lower right inset. An annual mean of 23.3 ± 25.8 Gt yr^{-1}, raging between a maximum loss of 78 Gt in 2003 and a minimum of 0.57 Gt in 2008 (Figure 6, inset A). It is important to highlight that, as the disintegration is computed from the surface area changes of each iceberg, part of the estimated potential freshwater input can be attributed to smaller icebergs fragmented from bigger ones and not to direct freshwater input.

Looking at the individual size classes, we computed a total mass loss as a function of area reduction of 9.3 Gt and 27 Gt for classes A2 and A3, respectively, followed by 84 and 132 Gt for A4 and A5. The average disintegration rates per year estimated for each size class were 64% (A2), 72% (A3), 14% (A4), and 38% (A5). The large disintegration rate estimated for A5 icebergs reinforces the occurrence of brittle fragmentation, which indicates that the mass loss resulting from those icebergs cannot be considered directly as freshwater input as part of it will continue drifting as 'child' icebergs born from those large ones.

Bransfield strait drift and freshwater input

Concerning Bransfield Strait (Figure 7), we detected the entrance of 13 icebergs class A2 with areas ranging between 1 and 5.5 km² between 2002 and 2005. The general drift pattern followed the ACoC circulation along with the complex topography near the tip of the Antarctic Peninsula. The integrated mass loss for the thirteen icebergs able to enter Bransfield Strait was estimated at 0.002 Gt day^{-1} (~0.19 Gt yr^{-1}), with an average disintegration rate of 38% yr^{-1} for all icebergs. The set of icebergs drifted on average 310 km from the northern Weddell Sea into Bransfield Strait at 3.4 ±1.1 km day^{-1} for about 95 days of observation. More icebergs were initially observed for the region, however, those icebergs were removed in the visual inspection due to not respecting a minimum number of

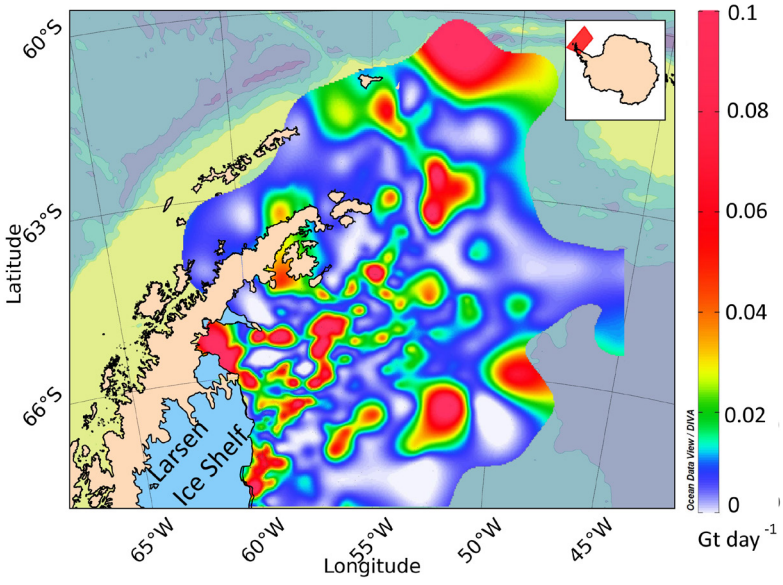

Figure 5. Spatial mass loss distribution (per day) for all iceberg trajectories between 2002 and 2010. Units are Gt day^{-1} on a log scale.

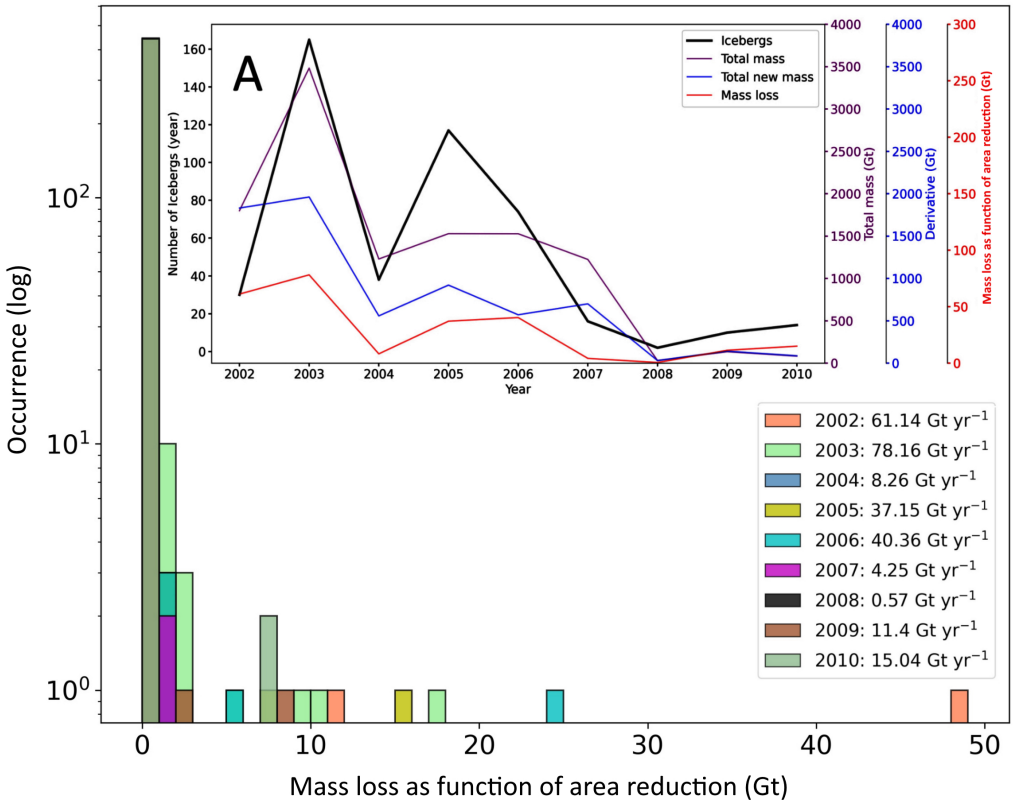

Figure 6. Integrated mass loss per year between 2002 and 2010. The histogram (log scale) relates the total occurrence (y-axis) of each iceberg mass loss estimated due to a reduction in surface area (x-axis). The annual mass loss estimated from area reduction between 2002 and 2010 is also shown in the lower right inset. Inset A presents the total number of icebergs (black line), total iceberg mass (purple line), total new mass (removed iceberg mass from previous years iceberg drifting; blue line) and, the total loss as a function of area reduction (red line) in the northwestern Weddell Sea sector.

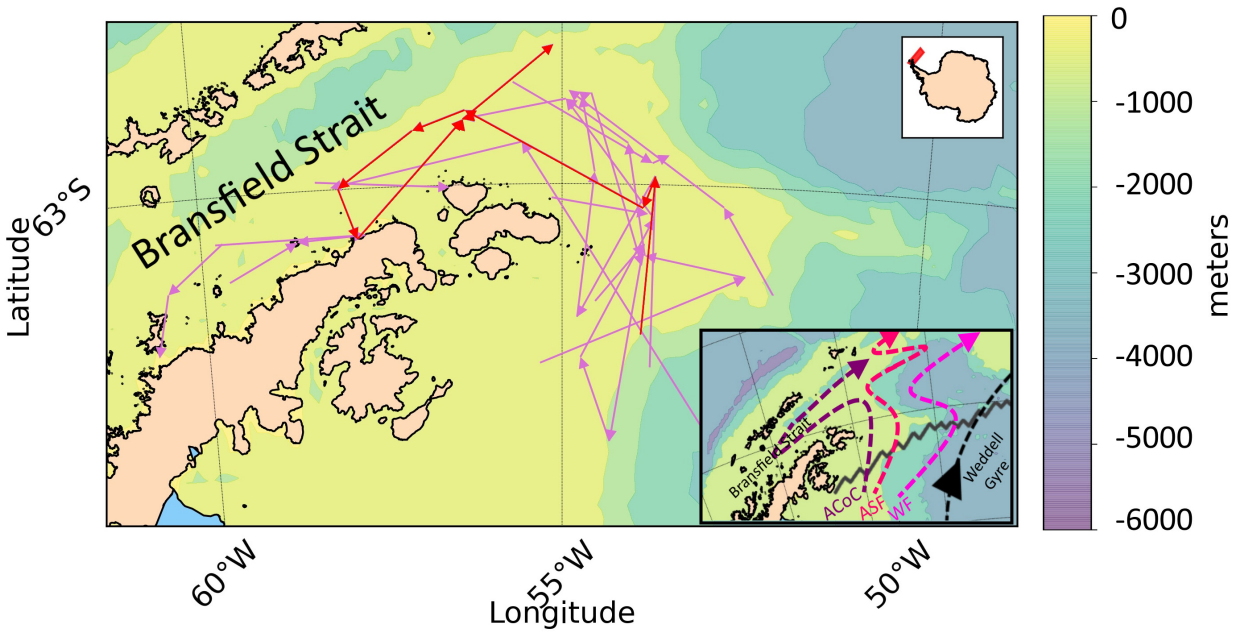

Figure 7. Icebergs entering the Bransfield Strait. A total of thirteen tracked icebergs are shown in purple. The trajectory of an iceberg with an initial area of 4.7 km^2 (drifting between July 2004 and December 2005) is highlighted in red. The main current circulation systems in the sector are shown in the bottom right corner inset. The color map depicts the bathymetry from the ETOPO database.

4 detections per trajectory or due to being impossible to validate redetection visually.

DISCUSSION AND CONCLUSIONS

Icebergs play a major role in freshwater transport and can be considered as a useful tool for tracing water movement on different routes along with the complex topography near the tip of the Antarctic Peninsula and the northwestern Weddell Sea. Nevertheless, only limited (in terms of minimum size/ ice coverage/modeling set up and parametrization) studies have addressed these issues to date. (Gladstone & Bigg 2002), using SAR imagery, manually tracked icebergs (200 m and 10 km across) in two areas of the Weddell Sea between January and February of 1992 and 1994. (Stuart & Long 2011b) using scatterometer data, limited to giant icebergs (> 18.5 km in length), presented the iceberg movement for the whole Antarctic coast. (Collares et al. 2018), based on a semi-automatic approach for iceberg detection and tracking, explored the drift dynamics of 25 icebergs with average surface areas of 9.06 ± 8,07 km^2 between 2008 and 2009. (Barbat et al. 2021), as a case study to demonstrate the applicability of an automatic tracking approach, tracked 414 icebergs for the whole Weddell Sea. From which 194 bergs (with surface areas between 3.4 km^2 and 2754 km^2) entered the northwestern Weddell Sea.

In this study, 450 free-drifting icebergs with surface areas ranging from 1 to 2765 km^2 were investigated, regarding prevalent trajectories and potential freshwater input across the northwestern Weddell Sea, from a total of 627 SAR images acquired between 2002 and 2010. We have applied autonomous methods based on machine learning and shape-based object recognition (Barbat et al. 2019a, 2021) to detect and track icebergs. The validation of tracked

iceberg positions (mainly for small size classes) is accomplished in this paper by correlating each automated detected iceberg position (per individual trajectory) with the expected presence of the same iceberg position into the sequence of SAR images, by visual inspection. An example is shown in Figure 2. A total accuracy (correctly detected trajectories/total detected trajectories) of 57.1% was computed for icebergs with a surface area smaller than 3.4 km^2 (76.4% for bigger ones). The tracking method accuracy results are usually directly related to the iceberg shape pattern. Icebergs with homogeneous shape contours make it difficult to build a reliable unidimensional shape signature able to be used to distinguish different icebergs, frequently merging distinct icebergs (and occasionally bright sea ice) as a single track (such bad tracks were removed from the analysis). To reduce the minimum iceberg area (accepted for tracking) from 3.4 to 1 km^2, we increased the confidence level between pair matches to 95% (previously 80%). Although the conservative strategy allowed to follow smaller icebergs with low shape variation between re-detection, the increase in confidence resulted in shorter trajectories (in time and trajectory length) and lower disintegration rates between pairs. For complete method details and validation, we recommend visiting (Barbat et al. 2019a, 2021).

The results yielded insights about the predominant iceberg (and, consequently, freshwater mass) northward transport associated with the bathymetric features and the main ocean circulation in the northwestern Weddell Sea. Although the observed icebergs followed predominantly the ACoC over the continental shelf on isobaths shallower than 500 m and also where the ASF and WF are dominant along the continental slope (about 3000 m), in agreement with observations (Stuart & Long 2011a, Collares et al. 2018) and model results (Merino et al. 2016, Rackow et al. 2017), larger icebergs spent a longer time inshore, increasing iceberg mass transport along the shallow areas due to direct input and/or brittle fragmentation. This can be related to shifts in the balance between the dominant forces for icebergs moving within the ACoC (wind drag, ocean drag and, "Coriolis-related force") (Gladstone et al. 2001). While smaller icebergs are more easily moved by catabatic winds, larger icebergs are mainly driven by currents under the influence of topographic features as suggested by (Stern et al. 2016). In addition, a small set of 13 icebergs with areas ranging from 1 to 5.5 km^2 were observed entering Bransfield Strait at the tip of the Antarctic Peninsula between 2002 and 2005, possibly, they were driven by the ACoC system following the potential vorticity contours (f/H). In this sense, some authors suggest a flow associated with both the ACoC and the ASF entering westward and recirculating eastward, influenced by the Bransfield Strait cyclonic circulation (Heywood et al. 1998, Zhou et al. 2002, Thompson et al. 2009, Caspel et al. 2018). Although not representative statistically, a single iceberg trajectory with an initial area of 4.7 km^2 was observed recirculating within Bransfield Strait between July 2004 and December 2005.

Concerning iceberg drift speeds, (Gladstone & Bigg 2002) estimated velocities of 4.3 km day^{-1} close to the Larsen Ice Shelf; from Argos tracking floats, (Schodlok et al. 2006) reported speeds below 9.5 ± 7.3 km day^{-1} in the western Weddell Sea; (Barbat et al. 2021) estimated 4.4 ± 8.3 km day^{-1} for 243 icebergs drifting along the Larsen Ice Shelf coming from about 72° South; following 25 icebergs through visual inspection, (Collares et al. 2018) computed speeds of ~7.9 ± 5,02 km day^{-1} in the northwestern Weddell Sea. In this study, we estimate an average speed of 3.4 ± 2.7 km day^{-1} for all 450 icebergs by class size: 2.2 ±1.5 km day^{-1} (A5), 2.5 ± 2.1 km day^{-1} (A4), 3.1 ± 3.2 km day^{-1} (A3) and, A2 iceberg with 3.8 ± 2.2 km day^{-1}.

Altogether, in agreement with the discussion by (Gladstone & Bigg 2002), there is a remarkable similarity between the average speeds closer to Larsen Ice Shelf, suggesting that both seasonal and interannual variability in mean iceberg trajectories and speeds may be small for that region. In addition, iceberg speed estimates across the Southern Ocean can vary as a result of geographical location and iceberg size (Gladstone & Bigg 2002, Schodlok et al. 2006, Merino et al. 2016, Rackow et al. 2017). However, for the northwestern Weddell Sea, where the sea ice cover is highly consolidated, it has been suggested that sea ice dominates those berg's movements, with wind forcing icebergs indirectly through an ice-floe steering mechanism (Lichey & Hellmer 2001) and/or in response to sea ice advance towards its maximum extension (Schodlok et al. 2006).

Analysis of the monitored trajectories suggests that most icebergs in the northwestern Weddell Sea follow the Weddell Gyre northward/eastward. Additionally, a few (13) small icebergs entered and might have recirculated in the Bransfield Strait. Altogether, it was estimated a potential freshwater input of 133.62 Gt yr^{-1} (at disintegration rate 62% yr^{-1}) for the northwestern Weddell Sea, and ~0.2 Gt yr^{-1} (at disintegration rate 38% yr^{-1}) for Bransfield Strait. It is important to note that, as shown above, class A2 icebergs (which includes all tracked icebergs into the Bransfield Strait) were tracked with a pair match confidence level of 95% due to the weak shape signature. As a consequence, those icebergs usually present reduced track length and period. This impacted our disintegration rate estimates, mainly due to major fracture/melting reshaping those icebergs beyond the accepted confidence interval. The direct annual mass loss as a function of area reduction between 2002 and 2010 is estimated to have an annual average of 23.3 ± 25.8 Gt yr^{-1}, ranging between 78 Gt in 2003 and 0.57 Gt in 2008. From the (Gladstone et al. 2001) estimate for an average calving rate in the Weddell Sea, (Schodlok et al. 2006) proposed that 31 Gt from the ~410 Gt annually calved are injected into the ocean as iceberg melt. Recent model-based simulations calculated a freshwater input between 153 and 589 Gt yr^{-1} for the whole Weddell Sea region (Merino et al. 2016, Rackow et al. 2017). In summary, although our results fit reasonably well with both discussions, freshwater estimates can be biased by the occurrence of brittle fragmentation from large icebergs, i.e. that part of the computed mass from area reductions is not immediately available as freshwater input to the ocean. The large disintegration rate estimated for A5 icebergs (38% yr^{-1}) reinforces the occurrence of brittle fragmentation. In addition, empirical relationships for estimating the iceberg keels and disintegration rates scaling (and freshwater flux) to a whole year may potentially lead to large uncertainties in the final computations. However, current state of art observing systems are still unable to overcome that difficulty.

Finally, the combination of machine learning and SAR imagery made it possible to follow 450 icebergs with surface areas between 1 to 2765 km^2, overcoming the usual iceberg tracking limitation to giant icebergs (>340 km^2), which often restricts iceberg monitoring via remote sensing. The main results reinforce the predominance of northward transport of icebergs in the northwestern Weddell Sea following the main currents along the Antarctic Peninsula, associated with the ACoC, ASF, and WF at an average drift speed of 3.4 ± 2.7 km day^{-1}. Only a few small icebergs entered and recirculated within Bransfield Strait. The average disintegration rate amounts to ~62% per year, leading to a potential freshwater input of 133.62 Gt yr^{-1} for all icebergs.

Acknowledgments

This study is a contribution to the activities of the Brazilian High Latitudes Oceanography Group (GOAL) and the Brazilian National Institute of Science and Technology of the Cryosphere (INCT-CRIOSFERA CNPq; 465680/2014-3). GOAL has been funded by the Brazilian Antarctic Program (PROANTAR) through the Ministério do Meio Ambiente (MMA), the Ministério da Ciência, Tecnologia e Inovações (MCTIC), the Conselho Nacional de Desenvolvimento Científico e Tecnológico (CNPq; 442628/2018-8), and Coordenação de Aperfeiçoamento de Pessoal de Nível Superior (CAPES) Foundation (AUXPE 1995/2014). M. M. Barbat acknowledges the fellowships from the Fundação de Amparo à Pesquisa do Estado do Rio Grande do Sul (INCT-Criosfera FAPERGS; 17/2551-0000518-0). M. M. Mata acknowledges CNPq grant 309653/2021-5. We also thank the European Space Agency (ESA) for providing the Envisat ASAR images used in this study and finally, two anonymous reviewer and Dr. Hartmut H. Hellmer for they attentive review and valuable suggestions. In addition, we have uploaded the full iceberg database and software used in this work to the institutional website of the Federal University of Rio Grande, Brazil (https://goal.furg.br/producao-cientifica/supplements).

REFERENCES

ÅSTRÖM JA. 2006. Statistical models of brittle fragmentation. Adv Phys 55: 247-278.

AZANEU M, KERR R, MATA MM & GARCIA CAE. 2013. Trends in the deep Southern Ocean (1958-2010): Implications for Antarctic Bottom Water properties and volume export. J Geophys Res Ocean 118: 4213-4227.

BARBAT MM, WESCHE C, WERHLI AV & MATA MM. 2019a. An adaptive machine learning approach to improve automatic iceberg detection from SAR images. ISPRS J Photogramm Remote Sens 156: 247-259

BARBAT MM, RACKOW T, HELLMER HH, WESCHE C & MATA MM. 2019b. Three Years of Near-Coastal Antarctic Iceberg Distribution From a Machine Learning Approach Applied to SAR Imagery. J Geophys Res Ocean 124: 6658-6672.

BARBAT MM, RACKOW T, WESCHE C, HELLMER HH & MATA MM. 2021. Automated iceberg tracking with a machine learning approach applied to SAR imagery: A Weddell sea case study. ISPRS J Photogramm Remote Sens 172: 189-206.

BARKER A, SAYED M & CARRIERES T. 2004. Determination of Iceberg Draft, Mass and Cross-Sectional Areas NRC Publications Archive (NPArC) Archives des publications du CNRC (NPArC) Determination of Iceberg Draft , Mass and Cross-Sectional Areas. Proc Int Offshore Polar Eng Conf.

BIGG GR, WADLEY MR, STEVENS DP, JOHNSON JA, SCIENCE CR, BIGG GR, WADLEY MR, STEVENS DP & JOHNSON JA. 1997. Modelling the dynamics and thermodynamics of icebergs. Cold Reg Sci Technol 26: 113-135.

CARTER L, MCCAVE IN & WILLIAMS MJM. 2008. Circulation and Water Masses of the Southern Ocean: A Review. Develop Earth Environ Sci 8: 85-114.

CASPEL MV, HELLMER HH & MATA MM. 2018. On the ventilation of Bransfield Strait deep basins. Deep Res Part II Top Stud Oceanogr 149: 25-30.

COLLARES LL, MATA MM, KERR R, ARIGONY-NETO J & BARBAT MM 2018. Iceberg drift and ocean circulation in the northwestern Weddell Sea, Antarctica. Deep Res Part II Top Stud Oceanogr 149: 10-24.

DAMINI BY, KERR R, DOTTO TS & MATA MM. 2021. Long-term changes on the Bransfield Strait deep water masses: Variability, drivers and connections with the northwestern Weddell Sea. Deep Sea Res Part I Oceanogr Res Pap 179: 103667.

DEPOORTER MA, BAMBER JL, GRIGGS JA, LENAERTS JTM, LIGTENBERG SRM, VAN DEN BROEKE MR & MOHOLDT G. 2013. Calving fluxes and basal melt rates of Antarctic ice shelves. Nature 502: 89-92.

DIETTERICH TG. 2000. Ensemble methods in machine learning. Lect Notes Comput Sci (including Subser Lect Notes Artif Intell Lect Notes Bioinformatics). 1857 LNCS: 1-15.

DOTTO TS, KERR R, MATA MM & GARCIA CAE. 2016. Multidecadal freshening and lightening in the deep waters of the Bransfield Strait, Antarctica. J Geophys Res Ocean.

ENDERLIN EM, HAMILTON GS, STRANEO F & SUTHERLAND DA. 2016. Iceberg meltwater fluxes dominate the freshwater budget in Greenland's iceberg-congested glacial fjords. Geophys Res Lett 43(11): 287-294.

ENVISAT/ESA HANDBOOK. 2007. ASAR Product Handbook, 564 p.

FAHRBACH E, ROHARDT G & KRAUSE G. 1992. The Antarctic coastal current in the southeastern Weddell Sea. Polar Biol 12: 171-182.

FERREIRA MLC & KERR R. 2017. Source water distribution and quantification of North Atlantic Deep Water and Antarctic Bottom Water in the Atlantic Ocean Prog Oceanogr 153: 66-83.

GLADSTONE R & BIGG GR. 2002. Satellite tracking of icebergs in the Weddell Sea. Antarct Sci 14: 278-287.

GLADSTONE RM, BIGG GR & NICHOLLS KW. 2001. Iceberg trajectory modeling and meltwater injection in the Southern Ocean. J Geophys Res Ocean 106: 19903-19915.

GORDON ALL. 2001. Bottom Water Formation. Encyclopedia of Ocean Sciences, p. 415-421.

HALE D. 2006. An efficient method for computing local cross-correlations of multi-dimensional signals. Color Sch Mines Consort Proj Seism Inverse Methods Complex Struct, p. 253-260.

HASS FS & JOKAR ARSANJANI J. 2020. Deep Learning for Detecting and Classifying Ocean Objects: Application of YoloV3 for Iceberg-Ship Discrimination. ISPRS Int J Geo-Information 9: 758.

HEYWOOD KJ, LOCARMINI RA, FREW RA, DENNIS PF & KING BA. 1998. Transport and water masses of the antarctic slope front system in the eastern weddell sea. Atmos Interact Antarct Cont Margin 75: 203-214.

IMPOCO G & TUMINELLO L. 2015. Incremental learning to segment micrographs. Comput Vis Image Underst 140: 144-152.

JACKA TH & GILES AB. 2007. Antarctic iceberg distribution and dissolution from ship-based observations. J Glaciol 53: 341-356.

JACOBS SS. 2004. Bottom water production and its links with the thermohaline circulation. Antarct Sci 16: 427-437.

JACOBS SS & HELLMER HH. 1992. Melting of ice shelves and the tnass balance of Antarctica. J Glaciol 38: 375-387.

KERR R, HEYWOOD KJ, MATA MM & GARCIA CAE. 2012. On the outflow of dense water from the Weddell and Ross Seas in OCCAM model. Ocean Sci 8: 369-388.

KOHN AF. 2005. Cross-correlation between EMG and center of gravity during quiet stance: Theory and simulations. Biol Cybern 93: 382-388.

LEE JS. 1981. Speckle analysis and smoothing of synthetic aperture radar images. Comput Graph Image Process 17: 24-32.

LICHEY C & HELLMER HH. 2001. Modeling giant-iceberg drift under the influence of sea ice in the Weddell Sea, Antarctica. J Glaciol 47: 452-460.

MARBACH D ET AL. 2012. Wisdom of crowds for robust gene network inference. Nat Methods 9: 796-804.

MARINO A, RULLI R, WESCHE C & HAJNSEK I. 2015. A new algorithm for iceberg detection with dual-polarimetric SAR data. Int Geosci Remote Sens Symp 2015-Novem, p. 3446-3449.

MAZUR AK, WÅHLIN AK & KRĘŻEL A. 2017. An object-based SAR image iceberg detection algorithm applied to the Amundsen Sea. Remote Sens Environ 189: 67-83.

MERINO N, LE SOMMER J, DURAND G, JOURDAIN NC, MADEC G, MATHIOT P & TOURNADRE J. 2016. Antarctic icebergs melt over the Southern Ocean : Climatology and impact on sea ice. Ocean Model 104: 99-110.

NICHOLLS KW, ØSTERHUS S, MAKINSON K, GAMMELSRØD T & FAHRBACH E. 2009. Ice-ocean processes over the continental shelf of the Southern Weddell Sea, Antarctica: A review Rev Geophys 47: 1-23.

NIWATTANAKUL S, SINGTHONGCHAI J, NAENUDORN E & WANAPU S. 2013. Using of Jaccard Coefficient for Keywords Similarity. Proc Int Multi Conference Eng Comput Sci.

ORSI AH, WHITWORTH T & NOWLIN WD. 1995. On the meridional extent and fronts of the Antarctic Circumpolar Current Deep. Res Part I 42: 641-673.

ORSI AH, JOHNSON GC & BULLISTER JL. 1999. Circulation, mixing, and production of Antarctic Bottom Water Prog Oceanogr. 43: 55-109.

PARKINSON CL & CAVALIERI DJ. 2012. Antarctic sea ice variability and trends, The Cryosph 6: 871-880.

POLIKAR R. 2006. Ensemble Based Systems in Decision Making. IEEE circuits Syst Mag.

PURKEY SG & JOHNSON GC. 2013. Antarctic bottom water warming and freshening: Contributions to sea level rise, ocean freshwater budgets, and global heat gain. J Clim 26: 6105-6122.

RACKOW T, WESCHE C, TIMMERMANN R, HELLMER HH, JURICKE S & JUNG T. 2017. A simulation of small to giant Antarctic iceberg evolution: Differential impact on climatology estimates. J Geophys Res Ocean 122: 3170-3190.

RANE A & SANGILI V. 2020. Implementation of Improved Ship-Iceberg Classifier Using Deep Learning. J Intell Syst 29: 1514-1522.

REZVANBEHBAHANI S, STEARNS LA, KERAMATI R, SHANKAR S & VAN DER VEEN CJ. 2020. Significant contribution of small icebergs to the freshwater budget in Greenland fjords. Commun Earth Environ 1: 1-7.

RIGNOT E, JACOBS S, MOUGINOT J & SCHEUCHL B. 2013. Ice-shelf melting around antarctica. Science 341: 266-270.

ROMANOV YA, ROMANOVA NA & ROMANOV P. 2008. Distribution of icebergs in the Atlantic and Indian ocean sectors of the

Antarctic region and its possible links with ENSO. Geophys Res Lett 35.

SANTISTEBAN J & TEJADA CARCAMO JL. 2015. Unilateral Jaccard similarity coefficient. CEUR Workshop Proc 1393: 23-27.

SCHODLOK MP, HELLMER HH, ROHARDT G & FAHRBACH E. 2006. Weddell Sea iceberg drift: Five years of observations. J Geophys Res Ocean 111: 1-14.

SILVA TAM & BIGG GR. 2005. Computer-based identification and tracking of Antarctic icebergs in SAR images. Remote Sens Environ 94: 287-297.

SILVA TAM, BIGG GR & NICHOLLS KW. 2006. Contribution of giant icebergs to the Southern Ocean freshwater flux. J Geophys Res Ocean 111: 1-8.

STARR A ET AL. 2021. Antarctic icebergs reorganize ocean circulation during Pleistocene glacials. Nature 589: 236-241.

STERN AA, ADCROFT A & SERGIENKO O. 2016. The effects of Antarctic iceberg calving-size distribution in a global climate model. J Geophys Res Ocean 121: 5773-5788.

STUART KM & LONG DG. 2011a. Iceberg size and orientation estimation using SeaWinds. Cold Reg Sci Technol 69: 39-51.

STUART KM & LONG DG. 2011b. Tracking large tabular icebergs using the SeaWinds Ku-band microwave scatterometer. Deep Res Part II Top Stud Oceanogr 58: 1285-1300.

SU Z, STEWART AL & THOMPSON AF. 2014. An Idealized Model of Weddell Gyre Export Variability. J Phys Oceanogr 44: 1671-1688.

THOMPSON AF, HEYWOOD KJ, THORPE SE, RENNER AHH & TRASVIÑA A. 2009. Surface circulation at the tip of the Antarctic Peninsula from drifters. J Phys Oceanogr 39: 3-26.

TOURNADRE J & TARASENKO A. 2019. Iceberg studies using satellite altimeter data. IEEE Inter Geoscience Remote Sens Symp, p. 3986-3989.

TOURNADRE J, BOUHIER N, GIRARD-ARDHUIN F & RÉMY F. 2016. Antarctic icebergs distributions 1992-2014. J Geophys Res Ocean 121: 327-349.

VORONTSOV IE, KULAKOVSKIY IV & MAKEEV VJ. 2013. Jaccard index based similarity measure to compare transcription factor binding site models. Algorith Mol Biol 8.

WESCHE C & DIERKING W. 2012. Iceberg signatures and detection in SAR images in two test regions of the Weddell Sea, Antarctica. J Glaciol 58: 325-339.

WILLIAMS RN, REES WG & YOUNG NW. 1999. A technique for the identification and analysis of icebergs in synthetic aperture radar images of Antarctica. Int J Remote Sens 20: 3183-3199.

ZHAN C, ZHANG L, ZHONG Z, DIDI-OOI S, LIN Y, ZHANG Y, HUANG S & WANG C. 2018. Deep Learning Approach in Automatic Iceberg - Ship Detection with SAR Remote Sensing Data. Int Geophysical conf, p. 24-27.

ZHANG G, DOVIAK RJ, VIVEKANANDAN J, BROWN WOJ & COHN SA. 2003. Cross-correlation ratio method to estimate cross-beam wind and comparison with a full correlation analysis. Radio Sci 38.

ZHOU M, NIILER PP & HU JH. 2002. Surface currents in the Bransfield and Gerlache Straits, Antarctica. Deep Res Part I Oceanogr Res Pap 49: 267-280.

How to cite

BARBAT MM & MATA MM. 2022. Iceberg drift and melting rates in the northwestern Weddell Sea, Antarctica: Novel automated regional estimates through machine learning. An Acad Bras Cienc 94: e20211586. DOI 10.1590/0001-3765202220211586.

Manuscript received on December 12, 2021;
accepted for publication on February 22, 2022

MAURO M BARBAT[1,2]
https://orcid.org/0000-0001-7930-1612

MAURICIO M MATA[1,2]
http://orcid.org/0000-0002-9028-8284

[1]Universidade Federal do Rio Grande – FURG, Laboratório de Estudos dos Oceanos e Clima (LEOC), Instituto de Oceanografia, Avenida Itália, Km 8, s/n, Campus Carreiros, 96203-900 Rio Grande, RS, Brazil

[2]Instituto Nacional de Ciência e Tecnologia da Criosfera, Grupo de Estudos do Oceano Austral e Gelo Marinho, Av. Itália, Km 8, 96203-900 Rio Grande, RS, Brazil

Correspondence to: **Mauro Medeiros Barbat**
E-mail: maurobarbat@furg.br

Author contributions

M. M. Barbat and M. M. Mata designed the study and analysis. M. M. Barbat developed the methods and led the writing of the original document. M. M. Mata contributed to reviewing and writing the manuscript.